Research Article

Journal of Environmental Nanotechnology

Green synthesis and Characterization of Zinc Oxide Nanoparticles Using *Ehretia laevis* Leaf Extract and Their Biological Evaluation

K. Vivek[1,2*], K. Abdhul[1], D. Mahendran[3], R. Manikandan[4], A. Karthick Kumar[2], K. Vishnukumari[2] and E. Thaniska[2]

[1]Department of Biotechnology, Nandha Arts and Science College (Autonomous), Erode, TN, India
[2]Department of Biotechnology, Sengunthar Arts and Science College (Autonomous), Tiruchengode, Namakkal, TN, India
[3]Department of Biotechnology, SRM Pavendar Bharathidasan College of Arts and Science, Pudukkottai, TN, India
[4]Department of Biotechnology, Rathinam College of Arts and Science, Coimbatore, TN, India
Received: 30.01.2026 Accepted: 14.02.2026 Published: 30.03.2026
*kvsvivek1994@gmail.com

ABSTRACT

The current study was conducted to encourage nanoparticle synthesis using zinc acetate in *Ehretia laevis* leaf extract, representing the first report of this plant for ZnO nanoparticle synthesis. UV, FTIR, SEM, EDX, XRD, and TGA analyses were conducted to characterize the structural properties of the nanoparticles. Additionally, the MTT test was conducted to determine the activity of cytotoxic zinc oxide nanoparticles (ZnO NPs). The biosynthesized ZnO NPs were preliminarily characterized by UV–visible spectroscopy, which revealed absorption features indicative of phytochemical interactions and ZnO nanoparticle formation. The XRD confirmed the hexagonal crystalline quartzite structure of the synthesized ZnO NPs. The morphology of the synthesized nanoparticles was examined by SEM, showing predominantly spherical to elliptical shapes, and their elemental composition was confirmed by EDX analysis. FTIR was used to confirm the functional groups responsible for stabilizing and capping ZnO NPs. The ZnO NPs exhibited a potent capacity to scavenge free radicals by DPPH scavenging potential. An IC_{50} value of 58.44 µg/mL indicated strong antioxidant activity. The cytotoxic effects of ZnO NPs on MDA-MB-231 human breast cancer cells were dose dependent, with an IC_{50} value of 38.81 µg/mL for nanoparticles. The synthesized ZnO NPs exhibited enhanced cytotoxic effects with increasing concentration, reaching a maximum at 100 µg/mL. The antioxidant and cytotoxic activities of ZnO nanoparticles synthesized using *E. laevis* make them a promising drug candidate for anticancer applications.

Keywords: Cytotoxicity; *Ehretia laevis*; MDA-MB-231 cells; Zinc oxide nanoparticles; Antioxidant activity.

1. INTRODUCTION

Breast cancer accounted for approximately 12 to 13 % of all new cancer cases globally in 2022, making it the most commonly diagnosed cancer among women worldwide. According to the World Health Organization and the International Agency for Research on Cancer, an estimated 2.3 million new cases and 670,000 deaths were reported in 2022, making breast cancer as the leading cancer among women in most countries (WHO, 2024; IARC, 2022). The lifetime risk of developing breast cancer is estimated to be 1 in 20 women worldwide, and the global burden is projected to increase to 3.2 million new cases annually by 2050, particularly in low- and middle-income regions (IARC, 2024).

Phytochemicals offer a viable treatment option due to their low cytotoxicity, accessibility, and prospective application as anticancer medications (Gulecha and Sivakuma, 2011). Numerous scientific studies have demonstrated the anticancer properties of phytochemicals. The survival and proliferation of malignant cells can be suppressed by disrupting their free radical scavenging mechanisms (Xiaoyan *et al*. 2018).

Ehretia laevis Roxb is a widely recognized medicinal herb used in traditional Indian medicine. Phytomedicine uses heartwood, leaves, bark, root system, branches, and fruits as conventional medicine. Due to their favorable responses to a variety of biological processes, such plants are utilized in many herbal and traditional treatments in China and India. Histological evidence of enhanced granulation, collagen deposition, and re-epithelialization indicates that *Ehretia laevis* Roxb leaf extract paste considerably improves wound healing when compared to topical phenytoin (Thakre *et al*. 2021). *E. laevis* have been used in Ayurvedic treatment of syphilis (Torane *et al.* 2009; Dhenge and Khandare, 2016). According to recent reports, *E. Laevis* extracts contain anti-inflammatory, antibacterial, antioxidant, and anti-

arthritic qualities (Jyothirmai *et al.* 2016). Interestingly, different phytoconstituents from different regions of *E. laevis* proved many kinds of pharmacological actions, such as low in glucose, anti-inflammatory in nature, cancer prevention, and hepatoprotective actions (Shukla and Kaur, 2018). Phytochemicals found in medicinal plants can serve as natural reducing, capping, and stabilizing agents in the environmentally friendly synthesis of metal oxide nanoparticles in addition to their therapeutic value. This creates a scientific connection between conventional phytomedicine and contemporary nanotechnology (Sugitha *et al.* 2024). Nanoparticles have been produced using environmentally friendly techniques using naturally occurring, non-toxic elements. The microscopic size of ZnO NPs facilitates their penetration and durability within tumorous cells, which aids in their activity. However, this also enhances the NPs' cellular utilization by cancerous cells, which eventually leads to cytotoxicity (Rasmussen *et al.* 2010). Silver nanoparticles have been synthesized using *Ehretia laevis* leaves (Panja *et al.* 2020; Syed and Ahmed, 2025). There are no reports existing for the synthesis of ZnO NPs using *Ehretia laevis*. Therefore, to the best of our knowledge, this is the first study to synthesize ZnO NPs using *Ehretia laevis* leaf extract *via* a green approach, followed by physicochemical characterization and also evaluation of their anticancer potential.

2. MATERIAL AND METHODS

2.1 Plant Extract Preparation

About 10 g of leaf powder was agitated and boiled for 30 minutes at 70 ℃ in 100 mL of distilled water. The extract was cooled to room temperature. The extract had a pH of 7.24. Whatman filter paper No. 1 was used for separating the resulting solution, which was then kept at 4 ℃ for later experimental use.

2.2 Green Synthesis of Zinc Oxide Nanoparticles

Zinc oxide nanoparticles were synthesized using the aqueous leaf extract of *Ehretia laevis*. First, 50 mM zinc acetate was dissolved in 100 mL of double-distilled water. From this solution, 90 mL was mixed with 10 mL of 10% aqueous *E. laevis* leaf extract under continuous magnetic stirring. The mixture was then subjected to ultrasonication at 450 Hz for 5 minutes, followed by stirring at 500 rpm until the solution became pale green, which indicated nanoparticle formation. The reaction mixture was allowed to settle, and the precipitate was collected by centrifugation at 3,000 rpm. The supernatant was further centrifuged at 15,000 rpm for 20 minutes to recover remaining nanoparticles. The collected nanoparticles were washed twice with 70% ethanol to remove impurities and then dried in an oven at 60 ℃ for further characterization.

2.3 UV- visible Spectral Analysis

The UV–visible absorption spectra of the synthesized ZnO NPs and the plant extract were recorded using a Shimadzu UV-2700 UV-visible spectrophotometer to confirm nanoparticle formation.

2.4 Fourier Transform Infrared (FTIR)

FTIR analysis was performed to identify the functional groups in the *Ehretia laevis* leaf extract responsible for the reduction and capping of the green-synthesized ZnO NPs. For analysis, 1 mg of ZnO NP powder was thoroughly mixed with 19 mg of KBr to prepare a fine homogeneous mixture. The mixture was then compressed into a pellet using a hydraulic press. FTIR spectra were recorded using an Agilent FTIR-Cary 630 spectrometer in the 400–4000 cm^{-1} range with a resolution of 4 cm^{-1}. The resulting spectra were analyzed to identify characteristic peaks corresponding to the functional groups involved in nanoparticle formation.

2.5 Scanning Electron Microscopy (SEM) and Energy-Dispersive X-ray (EDX)

The morphology and size of the green-synthesized ZnO NPs were examined using scanning electron microscopy (SEM). For SEM analysis, a small amount of dried ZnO NP powder was evenly sprinkled on an aluminum stub and coated with a thin layer of gold using a sputter coater to enhance conductivity. Micrographs were captured at different magnifications to observe nanoparticle shape and distribution. The average particle size was estimated by measuring at least 50 nanoparticles from ten randomly selected regions using AMT image analysis software. The elemental composition of the ZnO NPs was determined using energy-dispersive X-ray spectroscopy (EDX; Tokyo, Japan) attached to the SEM.

2.6 Thermal Characterization by TG DTA

The DTA-TG instrument (DTG-60H, Shimadzu Co., Japan) was used for the thermal gravimetric analysis (TGA). The sample was kept in a platinum crucible mounted on a microbalance pan and burned from the normal temperature to 700 ℃ with aluminum dioxide as a solvent. The test was conducted using N_2 flow and a rate of heating of 10 ℃/min.

2.7 X-ray Diffraction (XRD) Analysis

The crystalline structure of the green-synthesized ZnO nanoparticles was analyzed using X-ray diffraction (Philips X-ray diffractometer, Eindhoven,

Netherlands). Cu Kα radiation (λ = 1.540 Å) was used, with a voltage of 40 kV and a current of 30 mA. The diffraction patterns were recorded over a 2θ range of 10°–80°. The average crystallite size (D) of the nanoparticles was estimated using the Debye–Scherrer equation:

$$D = K\lambda / \beta\cos\theta \quad \ldots.(1),$$

where D is the mean crystallite size, K is the shape factor (0.9), λ is the X-ray wavelength, β is the full width at half maximum (FWHM) of the diffraction peak, and θ is the Bragg diffraction angle.

2.8 Antioxidant Activity

2.8.1 DPPH Radical Scavenging Activity

The 2,2-diphenyl-1-picrylhydrazyl (DPPH) assay was used to determine the antioxidant activity of the green-synthesized ZnO nanoparticles. DPPH was produced in a 0.1 mM methanol solution. Subsequently, 1 mL of DPPH solution and 1 mL of ZnO NP solutions at various concentrations (10–100 µg/mL) were mixed. Each mixture was allowed to incubate for half an hour at room temperature in the dark.

Standards and controls: Methanol without nanoparticles was used as the blank. The same amount of ascorbic acid was used as the positive control. All measurements were performed in triplicate to ensure reproducibility. Absorbance was determined at 517 nm on a UV-visible spectrophotometer.

Calculation:

$$\frac{Acontrol - Asample}{Acontrol} X\ 100 \quad \ldots (2)$$

where $A_{control}$ is the absorbance of the DPPH solution without sample, and A_{sample} is the absorbance in the presence of ZnO nanoparticles or a standard. Data were expressed as mean ± standard deviation (SD), and statistical analysis was performed using one-way ANOVA with $p < 0.05$ considered significant.

2.9 Cytotoxic Effect of ZnO NP

The cytotoxic potential of green-synthesized ZnO NPs was evaluated using the human breast cancer cell line MDA-MB-231 by the MTT assay. Cells were cultured in Dulbecco's Modified Eagle Medium (DMEM) supplemented with 10% fetal bovine serum (FBS) and 1% penicillin–streptomycin, and maintained at 37 °C in a humidified atmosphere containing 5% CO_2. Cells were seeded into 96-well plates at a density of 1×10^4 cells per well and allowed to attach overnight. After attachment, the culture medium was replaced with 100 µL of fresh DMEM containing ZnO NPs at concentrations ranging from 2 to 100 µg/mL. Control wells received medium without nanoparticles. Cells were incubated for 24 and 48 hours. Following incubation, 100 µL of MTT solution (0.5 mg/mL) was added to each well and the plates were incubated for 4 hours in the dark at 37 °C. The supernatant was then carefully removed, and the resulting formazan crystals were dissolved by adding 100 µL of dimethyl sulfoxide (DMSO) to each well, followed by gentle mixing for 10 min. Absorbance was measured at 570 nm using a microplate reader. Morphological changes were observed and documented using an inverted phase-contrast microscope (Nikon).

$$\text{Cell viability (\%)} = A_{control} / A_{sample} \times 100 \quad \ldots (3),$$

where:

- A_{sample} = absorbance of ZnO NP-treated cells
- $A_{control}$ = absorbance of untreated control cells

3. RESULTS AND DISCUSSION

3.1 UV-Vis Analysis



Fig. 1: Zinc oxide nanoparticles

3.2 FTIR Analysis of Biosynthesized ZnO NPs

Fig. 1 shows pale green precipitate generated with the incorporation of plant extract to the zinc acetate dihydrate precursor, signifying the phyto fabrication of

ZnO NPs following a 30-minute incubation period at room temperature. The UV–visible spectra of the plant extract and the biosynthesized ZnO nanoparticles are shown in Fig. 2. The plant extract exhibited a strong absorption peak at 260 nm, which can be attributed to π–π* transitions of phenolic and flavonoid compounds present in the extract. Following nanoparticle formation, an absorption peak at 262 nm was observed, indicating the involvement of plant-derived biomolecules in the reduction and stabilization of ZnO nanoparticles rather than intrinsic ZnO band-gap absorption. Similar absorption features in the 250–280 nm region have been reported for green-synthesized ZnO nanoparticles due to phytochemical capping (Iqtedar *et al*. 2020). Additionally, a broader absorption feature observed in the 350–380 nm region corresponds to the characteristic band-gap absorption of ZnO nanoparticles, confirming their formation, which is consistent with previous reports on biosynthesized ZnO NPs (Iqtedar *et al*. 2020; Singh *et al*. 2019).

The FTIR data of the extract and ZnO NPs are given in Table 1. The vibration peaks of extract (Fig. 3a) detected at 2921, 1769, 1583, 1513, 1445, 1383 and 1219 cm^{-1} are indicative of the corresponding functional group of carboxylic hydroxyl (OH), C=O ester, C=C aroma, NO_2 groups, CH_3 bending and C-OH stretching Nonetheless, the expected peak at approximately 2083 cm^{-1} is in line with the C–C stretching. ZnO NP spectrum shows vibrations at 3504, 2955, 2090, 1770, 1637, 1454, and 1375 cm^{-1} (Fig. 3b) corresponding to OH stretching of alcohol, OH stretching of carboxylic acid, C=C stretching, C=O aldehyde, C=C alkene, CH_2, and CH_3 bending. Additionally, it is firmly believed that phytochemicals, such as phenolic acids, are confirmed by the peaks in the region 1700-1600 cm^{-1}. The data reveal that the reducing agents of plants contain carboxylic acid. A distinctive peak was detected by the FT-IR at around 627 cm^{-1} (Zn-O stretching), indicating the formation of ZnO nanostructure, similar to one reported by Faye *et al*. (2022).

3.3 Morphology and composition of ZnO NPs

The surface morphology of the green-synthesized ZnO NPs was analyzed using SEM. The particles were predominantly quasi-spherical to irregular polyhedral in shape, with an average size in the range 70–100 nm (Fig. 4). The elemental composition was confirmed by EDX analysis (Fig. 5), which showed strong signals for Zn and O, verifying the formation of ZnO nanoparticles. Minor C signals were attributed to phytochemical capping agents from the plant extract, while trace Cu peaks likely originated from the copper sample holder used during SEM–EDX analysis.

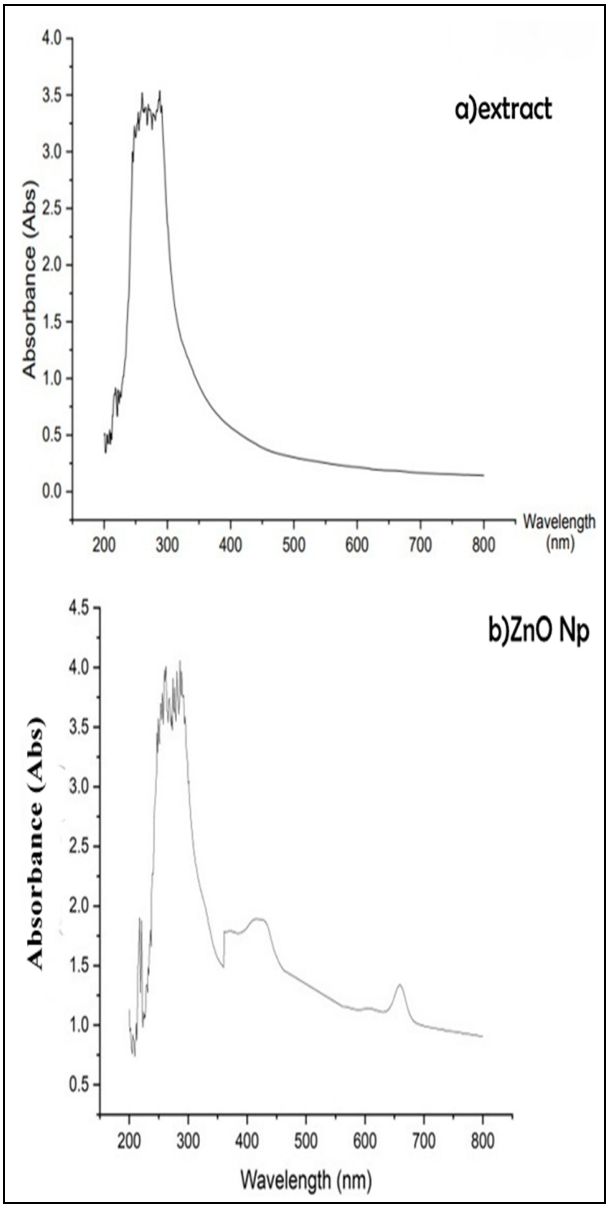


Fig. 2: UV-visible spectrum of $ZnSO_4$ reduction by leaf extract at 30 min

Table 1. FTIR spectra of ZnO NPs

Wavelength cm^{-1}	Leaf extract	Wavelength cm^{-1}	ZnO NPs
2921	O-H carboxylic acid	3504	OH stretching
1769	C=O ester	2955	OH carboxylic acid
1583	C=C aromatic	2090	C=C stretching
1513	NO_2 stretching	1770	C=O aldehyde
1445	C=C aromatic	1637	C=C alkene
1383	CH_3 bending	1454	CH_2 bending
1219	C-OH stretching	1375	CH_3 bending

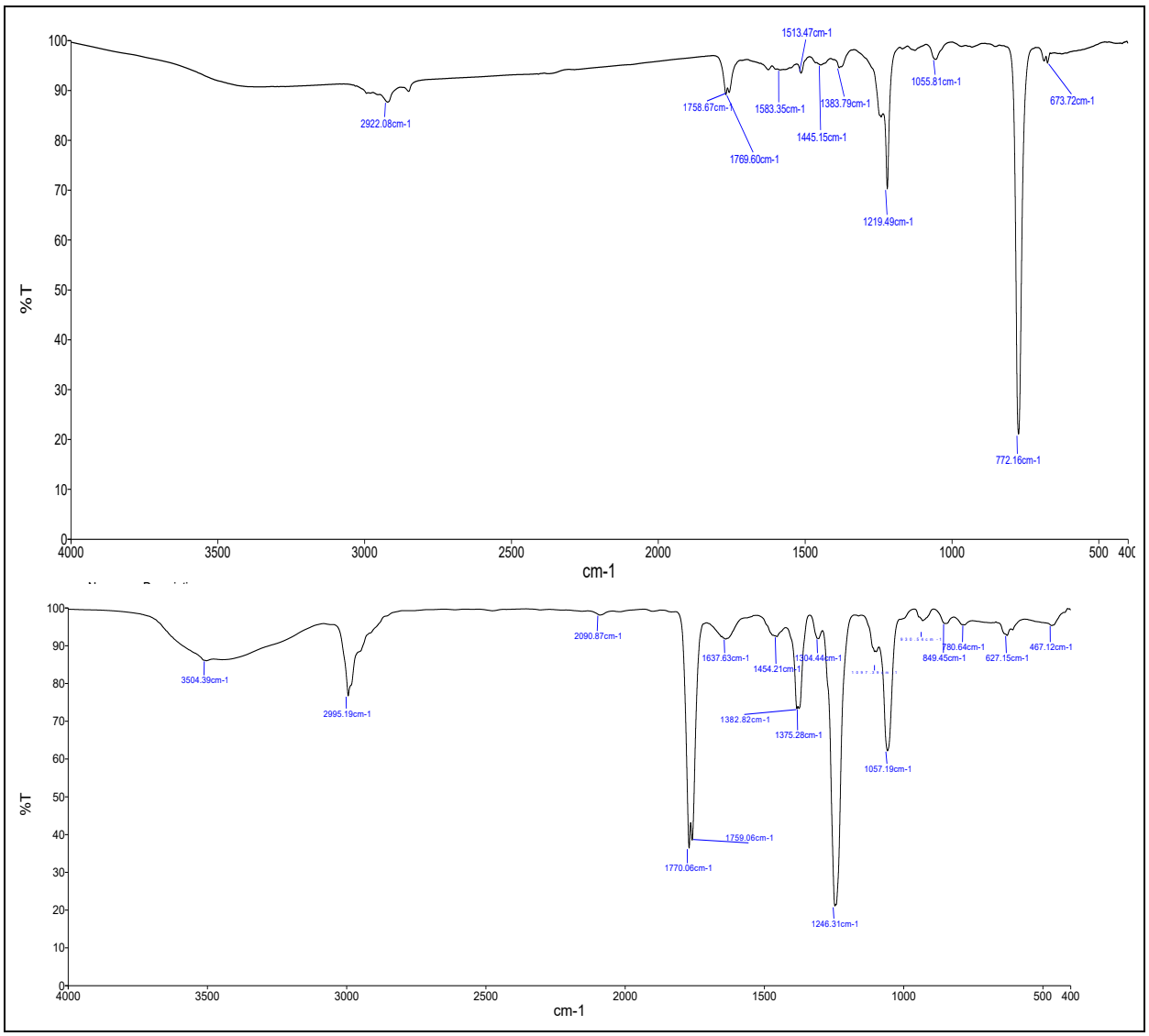


Fig. 3: FTIR spectra of (a) the extract and (b) ZnO NPs

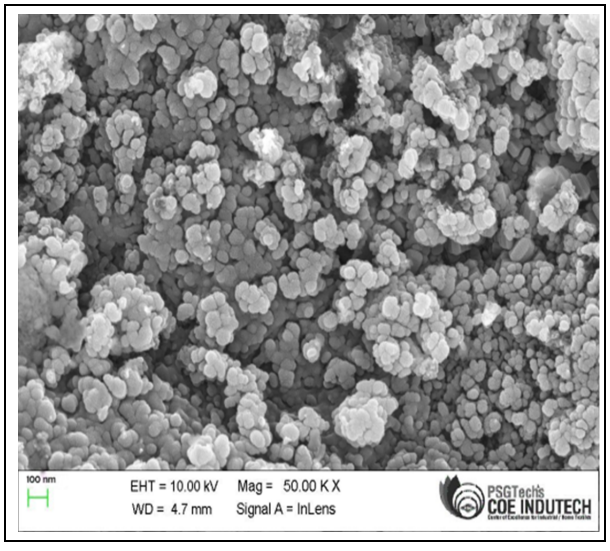


Fig. 4: SEM image of ZnO NPs (10X magnification)

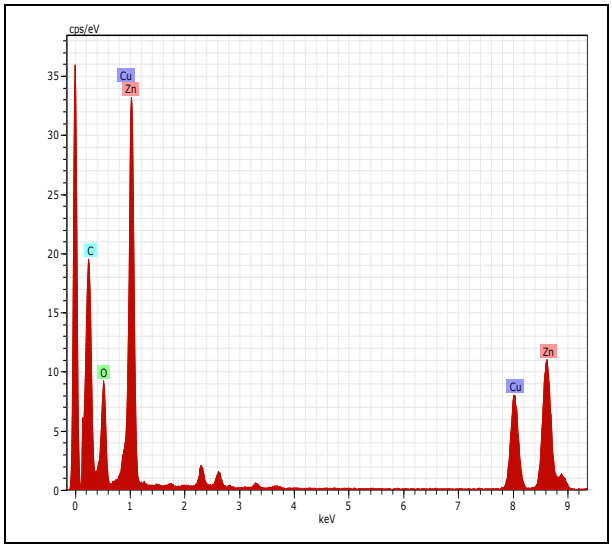


Fig. 5: EDAX plot of ZnO NPs

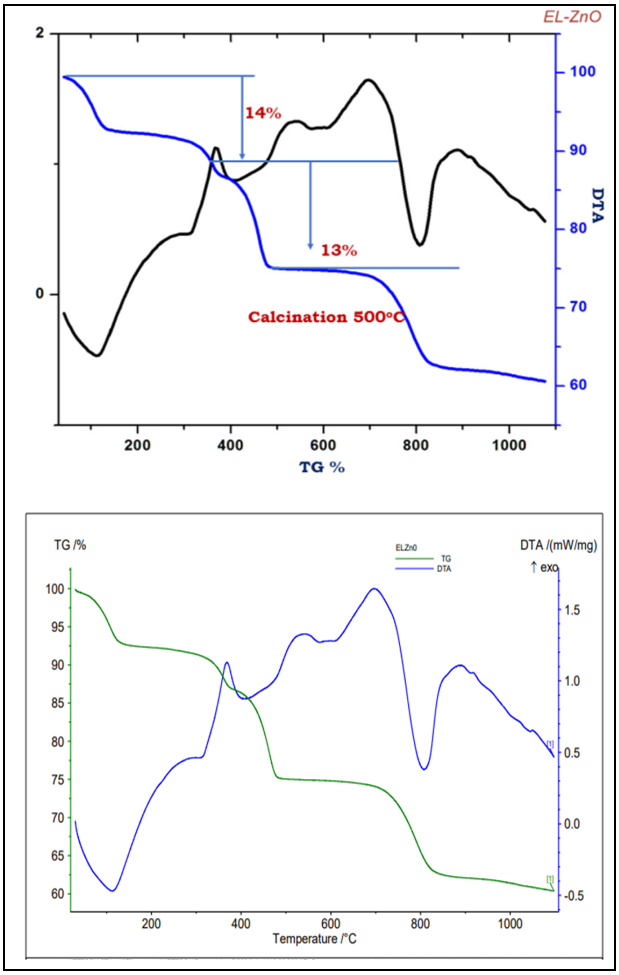


Fig. 6: (a) DT-TGA analysis of ZnO NPs and (b) calcination temperature of NPs

3.4 Thermal Characterization by TG DTA

Thermogravimetric analysis (TGA) was performed to evaluate the thermal stability of the green-synthesized ZnO NPs and to determine an appropriate calcination temperature. The TGA curve (Fig. 6a) showed a total weight loss of approximately 42% up to 800 °C, which can be attributed to the removal of moisture and decomposition of organic phytochemical residues. The initial weight loss observed between 250–400 °C (≈13%) is associated with the evaporation of adsorbed water and low-molecular-weight organic compounds. A second weight loss between 450–650 °C (≈14%) corresponds to the thermal decomposition of plant-derived capping agents. Beyond 650 °C, minimal weight change was observed, indicating improved thermal stability of the ZnO NPs. Based on these observations, a calcination temperature of 500 °C was selected as optimal to ensure effective removal of organic residues while preserving the structural integrity of ZnO NPs (Fig. 6b). The thermal stability observed is consistent with earlier reports on plant-mediated ZnO nanoparticles (Jan *et al*. 2020), although variations in total weight loss compared to other studies (Barzinjy and Azeez, 2020) may arise from differences in plant metabolites and synthesis conditions.

3.5 X-ray Diffraction Pattern of ZnO NPs

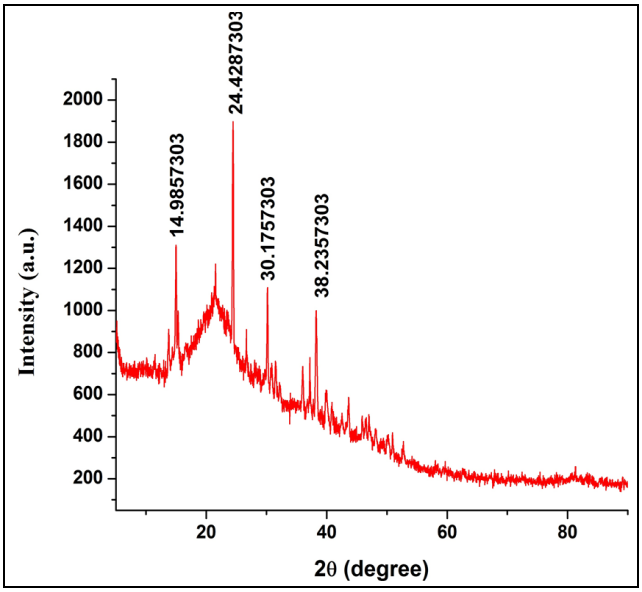


Fig. 7: XRD pattern of ZnO NPs dried at 100 °C

The X-ray diffraction pattern of synthesized Zn NPs is shown in Fig. 7. The diffraction peaks at 2θ angles of 38.20°, 30.17°, 24.42°, and 14.96°, correspond to reflections from the (111), (101), (200), and (001) crystal planes. The average FWHW was 40.776, and the particle measured 72 nm. Scherrer's formula was used to calculate the typical size of crystals of ZnO obtained from the FWHM of a more intense peak that corresponds to the 101 plane, which is hexagonal and is positioned at 36.28°. These angles are in accordance with the findings of the research conducted on the ZnO nanoparticle synthesized by Hashemi *et al.* 2016).

Table 2. Free radical scavenging activity of DPPH for ZnO nanoparticles

Concentration µg/ml	DPPH	Ascorbic Acid
10	17.91 + 1.53	22.01 + 0.93
20	24.70 + 1.56	30.25 + 1.06
30	26.53 + 1.11	34.49 + 1.29
40	32.75 + 1.33	40.21 + 1.05
50	37.08 + 0.93	48.39 + 1.04
60	44.34 + 0.77	56.55 + 1.23
70	62.68 + 1.55	70.24 + 0.86
80	67.36 + 1.01	82.46 + 0.77
90	72.49 + 1.55	88.29 + 0.75
100	87.73 + 1.76	95.29 + 0.96

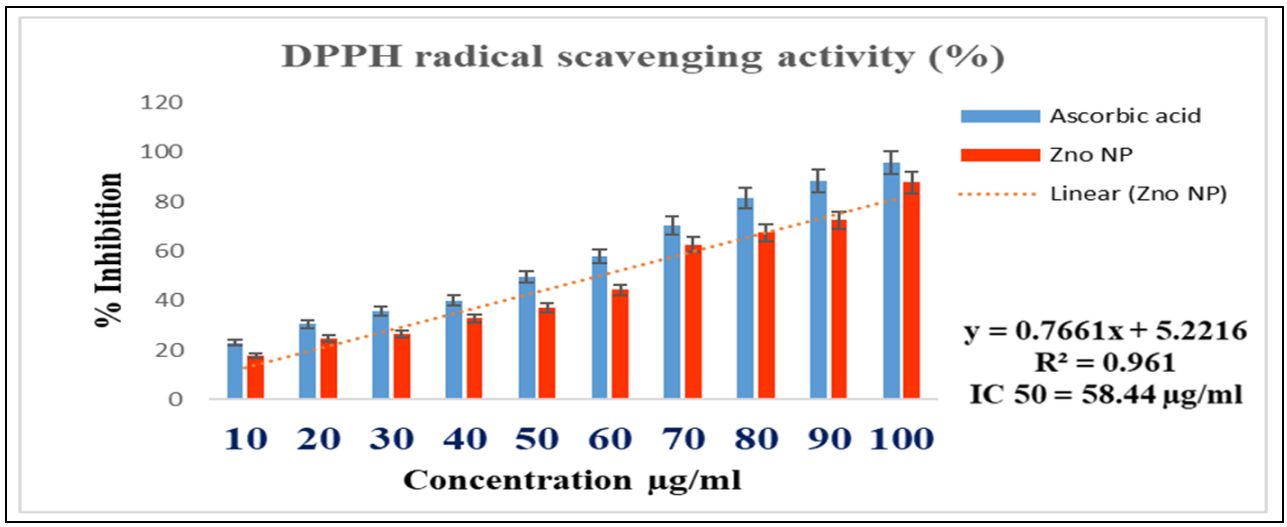


Fig. 8: DPPH activity of ZnO NPs and ascorbic acid

3.6 Antioxidant Activity of ZnO NPs

The antioxidant activity of the green-synthesized ZnO NPs was evaluated using the DPPH free radical scavenging assay at concentrations ranging from 10–100 µg/mL, with ascorbic acid used as the standard. All experiments were performed in triplicate, and results are expressed as mean ± standard deviation (SD) (Tables 2). A concentration-dependent increase in DPPH scavenging activity was observed for ZnO NPs (Fig. 8). At 10 µg/mL, ZnO NPs exhibited a scavenging activity of 17.91 ± 1.53%, which increased to 87.73 ± 1.76% at 100 µg/mL, with an IC_{50} value of 58.44 µg/mL. In comparison, ascorbic acid showed higher scavenging activity, increasing from 22.01 ± 0.93% at 10 µg/mL to 95.29 ± 0.96% at 100 µg/mL. The observed antioxidant activity is consistent with previous reports on ZnO nanoparticles synthesized using plant extracts (Mahendiran *et al.* 2017; Nagajyothi *et al.* 2015; Rehana *et al*. 2017; Abdelbaky *et al*. 2022).

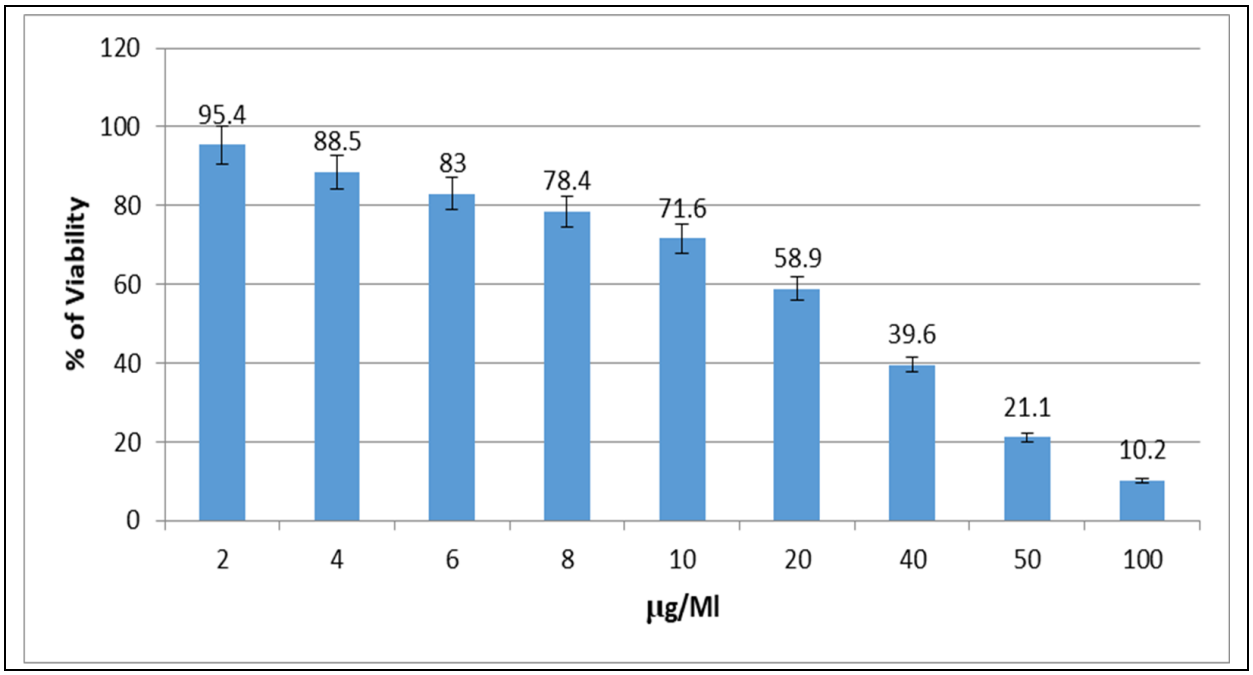


Fig. 9: MTT assay on MDA MB 231 at different concentrations for ZnO NPs

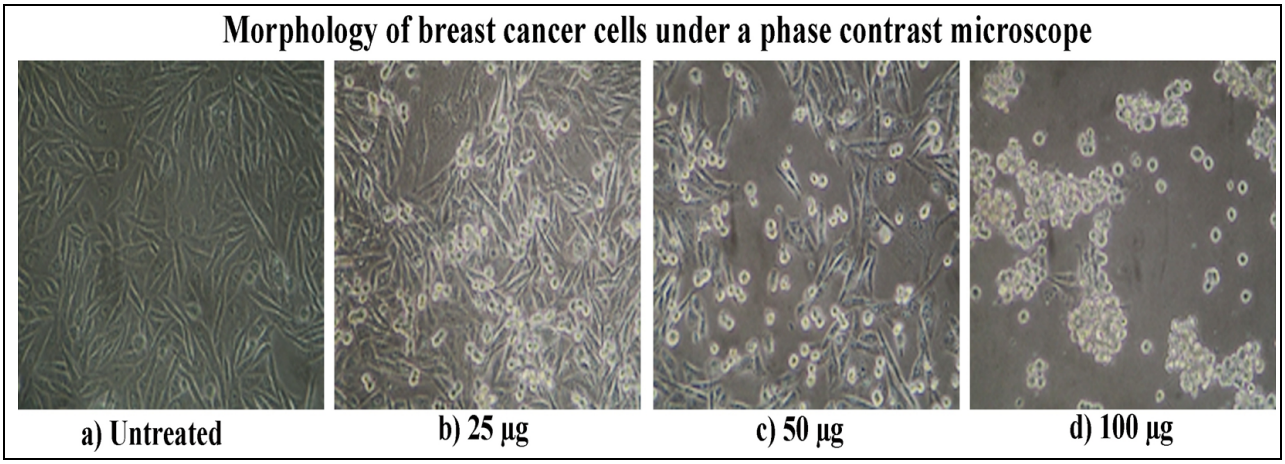


Fig. 10: Apoptotic cells under phase contrast

Table 3. Statistical analysis of cell viability treated with ZnO NP

Con µg/mL	2	4	6	8	10	20	40	50	100	Control
1	0.696	0.644	0.603	0.568	0.524	0.432	0.289	0.153	0.077	0.725
2	0.692	0.64	0.602	0.573	0.521	0.431	0.288	0.154	0.073	0.73
3	0.699	0.651	0.61	0.574	0.522	0.425	0.289	0.155	0.074	0.731
Mean OD	0.69567	0.645	0.605	0.571667	0.522333	0.429333	0.288667	0.154	0.074667	0.72867
SD	0.003512	0.005568	0.004359	0.00321455	0.001527525	0.003785939	0.00057735	0.001	0.002081666	0.003215
% of viability	95.47118	88.51784	83.02836	78.4538	71.68344	58.9204	39.61574	21.13449	10.24703	100

3.7 Cytotoxic Effect of ZnO NPs

The cytotoxicity of biosynthesized ZnO NPs against the cell line for human breast cancerous cell lines, MDA-MB-231 cells, was evaluated. After 48 hours of ZnO NPs treatment, the survival of human breast-derived cells was assessed. Fig. 9 indicates that the MDA-MB231 cancer cells react to increasing ZnO NPs concentrations. Death at 40 µg was measured at 39.61% after 48 hours of incubation, while at 50 µg, it reached 21.13%. At 100 µg, the cytotoxicity reached 10.24%. According to the dose-response curve, the concentration of ZnO NPs needed to reduce the proliferation of the cancerous cells in half is IC_{50} = 38.81 µg/mL. The finding is consistent with the outcomes of Lingaraju *et al* (2019). The capability of mitochondrial enzymes in living cells to change MTT to formazan is the basis for the MTT assay, which employs cellular respiration as a measure of cell survival and growth (Berridge *et al.* 2005). ZnO NPs-exposed cells displayed a concentration-dependent decline in survival after 48 hours of incubation; survival of cells is significantly reduced at concentrations between 40 and 100 µg. Fig. 10 shows the morphology of untreated and ZnO NPs-treated breast cancer cell lines under a phase contrast microscope. According to earlier research, green-produced ZnO NPs were less harmful to normal cells and exhibited excellent biocompatibility (Ebadi *et al.* 2019). Numerous investigations are showing that ZnO NPs have an excellent potential for cytotoxicity (Bisht and Rayamajhi, 2016).

4. CONCLUSION

In this study, zinc oxide nanoparticles were successfully green-synthesized using *Ehretia laevis* leaf extract. To the best of our knowledge, this is the first report describing the biosynthesis, physicochemical characterization, and biological evaluation of ZnO nanoparticles derived from *E. laevis*. The nanoparticles exhibited nanoscale size, crystalline wurtzite structure, thermal stability, antioxidant activity, and cytotoxic effects against MDA-MB-231 breast cancer cells, indicating their potential for further biomedical investigation.

ACKNOWLEDGMENTS

The authors are thankful to the Management of Nandha Arts and Science College for extending facilities and necessary support.

FUNDING

This research received no specific grant from any funding agency in the public, commercial, or not-for-profit sectors.

CONFLICTS OF INTEREST

The authors declare that there is no conflict of interest.

COPYRIGHT

This article is an open-access article distributed under the terms and conditions of the Creative Commons Attribution (CC BY) license (http://creativecommons.org/licenses/by/4.0/).

REFERENCES

Abdelbaky, A. S., Abd, M., Taia, A., Babalghith, A. O., Selim, S. and Mohamed, A. M. H. A., Green Synthesis and Characterization of ZnO Nanoparticles Using Pelargonium odoratissimum (L.) Aqueous Leaf Extract and Its Antioxidant, Antibacterial, and Anti-inflammatory Activities, *Antioxid.,* 11(8), 1444(2022). https://doi.org/10.3390/antiox11081444

Barzinjy, A. A. and Azeez, H. H., Green synthesis and Characterization of zinc oxide nanoparticles using Eucalyptus globulus Labill. Leaf extract and zinc nitrate hexahydrate salt, *SN Appl. Sci.,* 2(5), 991(2020). https://doi.org/10.1007/s42452-020-2813-1

Beiki, O., Hall, P., Ekbom, A. and Moradi, T., Breast cancer incidence and case fatality among 4.7 million women in relation to social and ethnic background: a population-based cohort study, *Breast Cancer Res.,* 14(1), 1–13 (2012). https://doi.org/10.1186/bcr3086

Berridge, M. V., Herst, P. M. and Tan, A. S., Tetrazolium dyes as tools in cell biology: new insights into their cellular reduction, *Biotechnol. Ann. Rev.,* 11, 127–152(2005). https://doi.org/10.1016/s1387-2656(05)11004-7

Bisht, G. and Rayamajhi, S., ZnO nanoparticles: a promising anticancer agent, *Nanobiomed.,* 3, 3–9 (2016). https://doi.org/10.5772/63437

Dhenge, S. and Khandare, K., Efficacy of local application of Khandu chakka (*Ehretia laevis* Roxb) Ghrita in Dushtavrana—A case report, *Int. J. Ayurveda Integr. Med.*, 4(12), 3726–3731 (2016).

Ebadi, M., Zolfaghari, M. R., Aghaei, S. S., Zargar, M., Shafiei, M., Zahiri, H. S., and Noghabi, K. A., A bio-inspired strategy for the synthesis of zinc oxide nanoparticles (ZnO NPs) using the cell extract of Cyanobacterium Nostoc sp. EA03: from biological function to toxicity evaluation, *RSC Adv.,* 9(41), 23508–23525 (2019). https://doi.org/10.1039/c9ra03962g

Faye, G., Jebessa, T. and Wubalem, T., Biosynthesis, Characterization and antimicrobial activity of zinc oxide and nickel doped zinc oxide nanoparticles using Euphorbia abyssinica bark extract, *IET Nanobiotechnol.,* 16(1), 25–32(2022). https://doi.org/10.1049/nbt2.12072

Ferlay, J., Ervik, M., Lam, F., Laversanne, M., Colombet, M. and Mery, L. *Global Cancer Observatory: Cancer Today*. International Agency for Research on Cancer. 2024 https://gco.iarc.fr/

Gulecha, V. and Sivakuma, T., Anticancer activity of Tephrosia purpurea and Ficus religiosa using MCF 7 cell lines, *Asian Pac. J. Trop. Med.,* 4(7), 526–529 (2011). https://doi.org/10.1016/S1995-7645(11)60139-9

Hashemi, S., Asrar, Z., Pourseyedi, S. and Nadernejad, N., Green synthesis of ZnO nanoparticles by Olive (Olea europaea), *IET Nanobiotechnol*., 10(6), 400–404(2016). https://doi.org/10.1049/iet-nbt.2015.0117

Iqtedar, M., Riaz, H., Kaleem, A., Abdullah, R., Aihetasham, A., Naz, S. and Sharif, S., Biosynthesis, optimization and Characterization of ZnO nanoparticles using Bacillus cereus MN181367 and their antimicrobial activity against multidrug-resistant bacteria, *Revista Mexicana de ingeniería química,* 19(1), 253–266(2020). https://doi.org/10.24275/rmiq/Bio1605

Jan, H., Shah, M., Usman, H., Khan, M. A., Zia, M., Hano, C., Abbasi, B. H., Biogenic synthesis and Characterization of antimicrobial and antiparasitic zinc oxide (ZnO) nanoparticles using aqueous extracts of the Himalayan Columbine (Aquilegia pubiflora), *Front. Mater.,* 7, 249(2020). http://dx.doi.org/10.3389/fmats.2020.00249

Jyothirmai, N., Nagaraju, B., Suresh, K,. J. N. and Swarupa, R. G., Evaluation of anti-inflammatory and anti-bacterial activities of different solvent extracts of *Ehretia laevis* Roxb, *J. Pharma. Sci. Res.,* 8(8), 715–720 (2016).

Kim, J., Harper, A., McCormack, V., Sung, H., Houssami, N., Morgan, E., Mutebi, M., Garvey, G., Soerjomataram, I., & Fidler-Benaoudia, M. M. (2025). Global patterns and trends in breast cancer incidence and mortality across 185 countries. *Nature Medicine,* 31(1154–1162). https://doi.org/10.1038/s41591-025-03502-3

Lingaraju, K., Naika, H. R., Nagabhushana, H. and Nagaraju, G., Euphorbia heterophylla (L.) mediated fabrication of ZnO NPs: Characterization and evaluation of antibacterial and anticancer properties, *Biocatal. Agric. Biotechnol.*, 18, 25 (2019) http://dx.doi.org/10.1016/j.bcab.2018.10.011

Mahendiran, D., Subash, G., Arumai, S. D., Rehana, D., Senthil, K. R., Kaliur, R. A., Biosynthesis of Zinc Oxide Nanoparticles Using Plant Extracts of Aloe vera and Hibiscus sabdariffa: Phytochemical, Antibacterial, Antioxidant and Anti-proliferative Studies, *BioNanoSci*., 7(3), 530–545(2017). https://doi.org/10.1007/s12668-017-0418-y

Nagajyothi, P. C., Sang, J. C., In, J. Y., Sreekanth, T. V. M., Kim, K. J. and Shin, H. M., Antioxidant and anti-inflammatory activities of zinc oxide nanoparticles synthesized using Polygala tenuifolia root extract, *J. Photochem. Photobio. B: Bio.*, 146, 10-17(2015). https://doi.org/10.1016/j.jphotobiol.2015.02.008

Panja, S., Choudhuri, I., Khanra, K., Pati, B. and Bhattacharyya, N., Biological and photocatalytic activity of silver nanoparticle synthesized from *Ehretia laevis* Roxb. leaves extract, *Nano Biomed. Eng.*, 12(1), 104-113 (2020).

Rasmussen, J. W., Martinez, E., Louka, P. and Wingett, D. G., Zinc oxide nanoparticles for selective destruction of tumor cells and potential for drug delivery applications, *Expert Opin. Drug Deliv.,* 7(9), 1063–77 (2010). https://doi.org/10.1517/17425247.2010.502560

Rehana, D., Mahendiran, D., Kumar, R. S., Kalilur, A. R., In vitro antioxidant and antidiabetic activities of zinc oxide nanoparticles synthesized using different plant extracts, *Bioprocess Biosyst. Eng.,* 40(6), 943–957 (2017). https://doi.org/10.1007/s00449-017-1758-2

Thakre, R., Arvinda Bhake., Pradip Tekade., Ketaki Harne., Preeti Sujit Borkar., Evaluation of *Ehretia Laevis* Roxb. (Khandu Chakka/Ajan Vruksha) in the Wound Healing Adjudged by Histological Examination of the Tissue, *Ind. J. Forensic Med. Toxicol.,* 15(2), 713-721(2021). https://doi.org/10.37506/ijfmt.v15i2.14397

Shukla, A. and Kaur, A., A systematic review of traditional uses bioactive phytoconstituents of genus Ehretia, *Asian J. Pharma. Clin. Res.,* 11, 88–100 (2018). https://doi.org/10.22159/ajpcr.2018.v11i6.25178

Siegel, R. L., Miller, K. D. and Jemal, A., Cancer statistics, *CA: Cancer J. Clinicians*, 68(1), 7–30 (2018). https://doi.org/10.3322/caac.21442

Sugitha, S. K. J., Latha, R. G., Venkatesan, R., Kim, S.-C., Vetcher, A. A. and Khan, M. R., Green Synthesis of Al-ZnO Nanoparticles Using *Cucumis maderaspatanus* Plant Extracts: Analysis of Structural, Antioxidant, and Antibacterial Activities. *Nanomater.*, 14(22), 1851(2024). https://doi.org/10.3390/nano14221851

Syed, I. J. and Ahmed, R. Z. Phytochemical Screening, Formulation and Optimization of *Ehretia Laevis* Loaded Silver Nanogel, *Res. Square*., 1-35 (2025).

Torane, R. C., Ruikar, A. D., Chandrachood, P. S. and Deshpande, N. R., Study of amino acids and carbohydrates from the leaves of *Ehretia laevis*, *Asian J. Chem.,* 21(2), 1636–1638 (2010).

World Health Organization. (2025, August 14). *Breast cancer: Fact sheet*. https://www.who.int/news-room/fact-sheets/detail/breast-cancer

Xiaoyan, Y., Xie, T., Wang, S. D., Wang, Z., Li, H. Y. and Zhaoming, Y., Apigenin inhibits proliferation of human chondrosarcoma cells via cell cycle arrest and mitochondrial apoptosis induced by ROS generation-an in vitro and in vivo study, *Int. J. Clin. Exp. Med*, 11(3), 1615–1631 (2018). https://api.semanticscholar.org/CorpusID:49365619